

## Analysis of dielectric loaded surface plasmon waveguide structures: Transfer matrix method for plasmonic devices

Xiao Yong He, Qi Jie Wang, and Siu Fung Yu

Citation: *J. Appl. Phys.* **111**, 073108 (2012); doi: 10.1063/1.3703468

View online: <http://dx.doi.org/10.1063/1.3703468>

View Table of Contents: <http://jap.aip.org/resource/1/JAPIAU/v111/i7>

Published by the [American Institute of Physics](http://www.aip.org).

---

### Related Articles

Two-dimensional Bessel-like surface plasmon-polariton beams

*J. Appl. Phys.* **112**, 103107 (2012)

High-efficiency spoof plasmon polariton coupler mediated by gradient metasurfaces

*Appl. Phys. Lett.* **101**, 201104 (2012)

Buried anti resonant reflecting optical waveguide based on porous silicon material for an integrated Mach Zehnder structure

*Appl. Phys. Lett.* **101**, 191114 (2012)

A quantum dot rolled-up microtube directional coupler

*Appl. Phys. Lett.* **101**, 171111 (2012)

Lithium niobate photonic crystal wire cavity: Realization of a compact electro-optically tunable filter

*Appl. Phys. Lett.* **101**, 151117 (2012)

---

### Additional information on *J. Appl. Phys.*

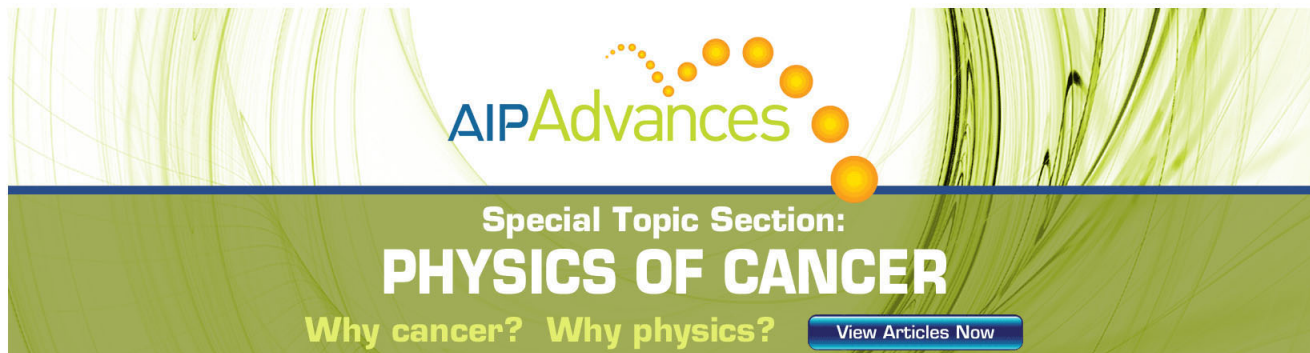
Journal Homepage: <http://jap.aip.org/>

Journal Information: [http://jap.aip.org/about/about\\_the\\_journal](http://jap.aip.org/about/about_the_journal)

Top downloads: [http://jap.aip.org/features/most\\_downloaded](http://jap.aip.org/features/most_downloaded)

Information for Authors: <http://jap.aip.org/authors>

## ADVERTISEMENT



**AIP Advances**

Special Topic Section:  
**PHYSICS OF CANCER**

Why cancer? Why physics? [View Articles Now](#)

# Analysis of dielectric loaded surface plasmon waveguide structures: Transfer matrix method for plasmonic devices

Xiao Yong He,<sup>1</sup> Qi Jie Wang,<sup>1,2,a)</sup> and Siu Fung Yu<sup>3</sup>

<sup>1</sup>*School of Electrical and Electronic Engineering, Nanyang Technological University, Singapore, 639798*

<sup>2</sup>*School of Physical and Mathematical Sciences, Nanyang Technological University, Singapore, 637371*

<sup>3</sup>*Department of Applied Physics, Hong Kong Polytechnic University, Kowloon, Hong Kong*

(Received 15 November 2011; accepted 13 March 2012; published online 11 April 2012)

The propagation properties of dielectric loaded surface plasmon polariton (DLSPP) waveguide structures have been investigated by using the transfer matrix method (TMM), which is simple and has a fast calculation speed. The results obtained from the TMM agree well with those from the finite element method. As a demonstration, we investigate the waveguide properties of DLSPP structures in the terahertz and near-infrared regimes. The TMM is potentially a powerful and effective tool for studying various plasmonic waveguide structures, which may find important applications in integrated photonic devices and sensors. © 2012 American Institute of Physics. [<http://dx.doi.org/10.1063/1.3703468>]

## I. INTRODUCTION

Surface plasmon polaritons (SPPs) are two-dimensional (2D) electromagnetic waves confined at the metal–dielectric interfaces, with electric field components decaying exponentially into the neighboring media.<sup>1</sup> They can be used to break the diffraction limit, which is very important and useful for fabrication of integrated miniaturized optical circuits.<sup>2–5</sup> Up to now, different kinds of SPP waveguides have been proposed, such as the hybrid plasmonic waveguide,<sup>6,7</sup> the channel plasmonic structures,<sup>8</sup> the gap SPPs waveguide,<sup>9,10</sup> and the dielectric loaded surface plasmon polaritons (DLSPP) waveguide.<sup>11,12</sup> The DLSPP waveguide demonstrates strong lateral confinement, low edge-scattering and low bending losses, resulting in a high integration density of components, and can be fabricated with the present industrial photolithography techniques.<sup>13</sup> Compared with other SPP waveguides, the dielectric core of the DLSPP waveguide structures can be easily designed to include an active medium<sup>14</sup> with gain and to achieve a high index contrast between the dielectrics and air.

So far, the DLSPP waveguide has been studied both experimentally<sup>14–16</sup> and theoretically,<sup>17</sup> and used for various plasmonic devices, e.g., thermal tunable filters,<sup>18</sup> splitters,<sup>19</sup> and resonators. From the experimental aspect, for example, the propagation losses of the DLSPP waveguides were reduced by doping the dielectric layer with quantum dots or rare earth ions.<sup>14</sup> From the theoretical aspect, the DLSPP waveguide can be treated as an asymmetric slab structure, the propagation properties of which were investigated by solving the eigenvalue equation.<sup>20</sup> Several other numerical methods, such as the finite element method (FEM), the finite-difference time-domain (FDTD) method,<sup>17</sup> the Green's function method,<sup>21</sup> the differential method, and the multi-domain pseudospectral method,<sup>22</sup> have been developed to investigate the propagation properties of the DLSPP waveguide. However, these numerical techniques have the disadvantages of involving rigorous and

time-consuming calculations, and high demand for memory. With the rapid development of plasmonic devices,<sup>23</sup> it is highly desired to have a simple and high efficient calculation method for investigating DLSPP waveguides, and broadly extendable to plasmonic devices.

In this work, we propose to apply transfer matrix method (TMM), which has the advantages of simplicity and high efficiency as compared to the FEM and FDTD methods, for the design of DLSPP structures. Due to the weak optical confinement in the DLSPP waveguides, the full-width-half-maximum (FWHM) of the optical mode is chosen as the effective optical mode width for numerical calculations in the TMM. As a result, the calculation accuracy of permittivity based on the TMM is similar to that calculated from the FEM, but the calculation speed of the TMM is significantly shorter.

Recently, most of the research about DLSPP waveguides has been concentrated in visible<sup>12</sup> and infrared,<sup>18</sup> spectral ranges. Little work has been carried out in the terahertz (THz) regime, which is also an important spectral range with many important applications.<sup>24–26</sup> The lack of suitable waveguide design methods and waveguide devices greatly hinder the development of THz technology.<sup>27–31</sup> Because the DLSPP waveguide has the merits of subwavelength confinement and strong guiding properties, it shows great potentials in fabricating THz waveguide devices, such as resonators, splitters, and sensors. In this paper, the propagation properties of DLSPP structures in the infrared and THz regimes have been investigated by using the proposed TMM technique. The performance of the plasmonic devices obtained from the TMM is comparable to that obtained from the FEM. The presented work demonstrates that the TMM is a promising technique to study the propagation properties of DLSPP waveguides, and potentially it is more broadly applicable to other plasmonic devices.

## II. THEORETICAL MODEL AND METHOD

Figure 1 shows the schematic structure of the DLSPP waveguide, which is formed by a dielectric stripe deposited

<sup>a)</sup>Author to whom correspondence should be addressed. Electronic mail: [qjwang@ntu.edu.sg](mailto:qjwang@ntu.edu.sg).

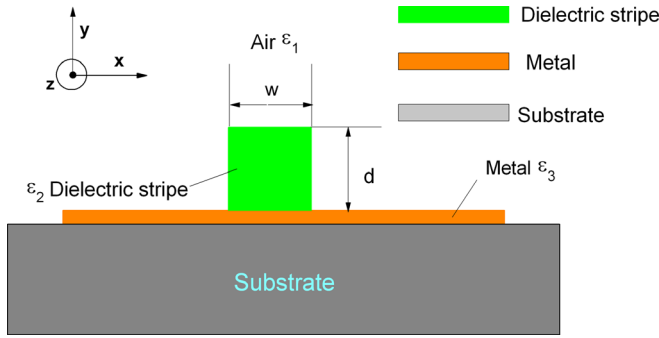


FIG. 1. Schematic structures of the cross section of DLSPPs waveguide. The width and the thickness of the dielectric stripe are  $w$  and  $d$ , respectively.

on a metal or a heavily doped semiconductor surface. The dielectric ridge has a thickness of  $d$  in the  $y$  direction and a width of  $w$  in the  $x$  direction. For the DLSPP asymmetric slab structure, the field components for transverse magnetic (TM) waves can be expressed as follows:<sup>32</sup>

$$H_x = e^{-\gamma_1 y}, \quad 0 < y < \infty, \quad (1)$$

$$H_x = [\cos \gamma_2 y - (\varepsilon_2/\varepsilon_1)(\gamma_1/\kappa)\sin \gamma_2 y], \quad -d < y < 0, \quad (2)$$

$$H_x = [\cos \gamma_2 d + (\varepsilon_2/\varepsilon_1)(\gamma_1/\gamma_2)\sin \gamma_2 d] \times \exp[\gamma_3(y + d)], \quad -\infty < y < -d, \quad (3)$$

where

$$\gamma_j^2 = \beta^2 - k_0^2 \varepsilon_j, \quad i = 1, 2, 3, \quad (4)$$

$\beta$  is the propagation constant of the surface mode, and  $k_0$  is the wave vector in vacuum. The corresponding  $E_y$  and  $E_z$  are given as  $E_y = (i/\varepsilon_i \omega \varepsilon_0)(\partial H_x / \partial z)$  and  $E_z = -(i/\varepsilon_i \omega \varepsilon_0)(\partial H_x / \partial y)$ , respectively.

The asymmetric slab DLSPP waveguide structures can also be investigated by solving the eigenvalue equation. By applying the boundary conditions (the tangential  $E$  field is continuous at  $x=0$ ), the transcendental equation can be expressed as<sup>32</sup>

$$k_0 d = (\varepsilon_2 - n_{\text{eff}}^2)^{-1/2} \left\{ \tan^{-1} \frac{\varepsilon_2}{\varepsilon_1} \left[ \frac{n_{\text{eff}}^2 - \varepsilon_1}{\varepsilon_2 - n_{\text{eff}}^2} \right]^{1/2} + \tan^{-1} \frac{\varepsilon_2}{\varepsilon_3} \left[ \frac{n_{\text{eff}}^2 - \varepsilon_3}{\varepsilon_2 - n_{\text{eff}}^2} \right]^{1/2} + \nu \pi \right\}, \quad (5)$$

where  $\nu$  is the mode number.

The propagation properties of the DLSPP structures in 2D can be solved by dividing the cross section of the DLSPP waveguide into two one-dimensional structures. First, along the  $y$  direction the propagation constant of the guided waves  $\beta_{\text{eff}}^y$  are calculated. In this case, there are four layers from the bottom to the top, consisting of the substrate, the metal, the dielectric stripe, and the air. Second, the overall effective indices of the DLSPP modes are obtained from the three-layer structure along the  $x$  direction, consisting of the air, the dielectric stripe and the air, starting from the left to the right. In this calculation, the effective indices of  $\beta_{\text{eff}}^y$  and  $n_{\text{spp}}$

(the effective indices of the SPP modes propagating along the metal–air interface) are used.

TMM is often used to calculate the propagation constants of the multilayer structures.<sup>33</sup> For TM modes, imposing the boundary conditions at the interface between  $i$ th layer and  $(i+1)$ th layer lead to the following equations:<sup>34</sup>

$$(H_{i+1}^+ + H_{i+1}^-)_{i,i+1} = (H_i^+ + H_i^-)_{i,i+1}, \quad (6)$$

$$\frac{\gamma_{i+1}}{\varepsilon_{i+1}} (H_{i+1}^+ - H_{i+1}^-)_{i,i+1} = \frac{\gamma_i}{\varepsilon_i} (H_i^+ - H_i^-)_{i,i+1}, \quad (7)$$

where  $H_i^+$  and  $H_i^-$  are the magnetic fields of the propagation and the reflected waves in the  $i$ th layer, respectively. From Eqs. (6) and (7), the field coefficients between  $i$ th and  $(i+1)$ th layers can be written as

$$\gamma_{i+1} \varepsilon_i \begin{bmatrix} H_{i+1}^+ \\ H_{i+1}^- \end{bmatrix}_{i,i+1} = \frac{1}{2} \begin{bmatrix} \varepsilon_i & \varepsilon_{i+1} \\ \varepsilon_i & -\varepsilon_{i+1} \end{bmatrix} \begin{bmatrix} \gamma_{i+1} & \gamma_{i+1} \\ \gamma_i & -\gamma_i \end{bmatrix} \begin{bmatrix} H_i^+ \\ H_i^- \end{bmatrix}_{i,i+1}, \quad (8)$$

$$\begin{bmatrix} H_i^+ \\ H_i^- \end{bmatrix}_{i,i+1} = \begin{bmatrix} \exp(\gamma_i d_i) & 0 \\ 0 & \exp(-\gamma_i d_i) \end{bmatrix} \begin{bmatrix} H_i^+ \\ H_i^- \end{bmatrix}_{i-1,i}, \quad (9)$$

in which  $d_i$  is the thickness of the  $i$ th layer. Thus, the relation between the magnitude of the magnetic field of incident waves at the first layer and that of the reflected waves at the last layer can be expressed in the following transfer matrix form:

$$\gamma_2 \gamma_3 \cdots \gamma_N \varepsilon_1 \varepsilon_2 \cdots \varepsilon_{N-1} \begin{bmatrix} H_N^+ \\ H_N^- \end{bmatrix}_{N,N-1} = \begin{pmatrix} M_{11} & M_{12} \\ M_{21} & M_{22} \end{pmatrix} \begin{bmatrix} H_1^+ \\ H_1^- \end{bmatrix}_{1,1}, \quad (10)$$

where  $H_N^+$  and  $H_N^-$  are the magnetic fields of the propagation and the reflected waves in the  $N$ th layer, respectively. The matrix product of characteristic matrices can be written as

$$\begin{pmatrix} M_{11} & M_{12} \\ M_{21} & M_{22} \end{pmatrix} = M_{N-1} M_{N-2} \cdots M_i \cdots M_1, \quad (11)$$

where  $M_i$  is the characteristic matrices in the  $i$ th layer,

$$M_i = \begin{pmatrix} \varepsilon_{i-1} & \varepsilon_i \\ \varepsilon_{i-1} & -\varepsilon_i \end{pmatrix} \begin{pmatrix} \gamma_i & \gamma_i \\ \gamma_{i-1} & -\gamma_{i-1} \end{pmatrix} \begin{pmatrix} \exp(\gamma_i d_i) & 0 \\ 0 & -\exp(\gamma_i d_i) \end{pmatrix}. \quad (12)$$

InSb is a narrow gap semiconductor and has a high intrinsic electron density at room temperature, which displays metallic characteristics in the THz regime. The permittivity of doped semiconductor in the THz regime can be written as<sup>35</sup>

$$\varepsilon(\omega) = \left( \varepsilon_\infty - \frac{\omega_p^2}{\omega^2 + \omega_\tau^2} \right) + i \frac{\omega_\tau \omega_p^2}{\omega(\omega^2 + \omega_\tau^2)}, \quad (13)$$

where  $\omega_p$  and  $\omega_\tau$  are the plasma and damping frequencies, respectively. The values of  $\omega_p$  and  $\omega_\tau$  change with different

temperatures and carrier concentration  $\omega_p = \sqrt{n_d e^2 / \epsilon_\infty \epsilon_0 m^*}$ ,  $\omega_\tau = 1 / (\mu \cdot m^* / e)$ , in which  $m^*$  is the effective mass,  $\mu$  is the mobility of the electron,  $n_d$  is the carrier concentration, and  $e$  is the electronic charge. The intrinsic carrier concentration of InSb between 200 and 798 K can be well described by the following formula:<sup>36</sup>

$$n_d = 2.9 \times 10^{11} (2400 - T)^{0.75} (1.0 + 2.7 \times 10^{-4} T) T^{1.5} \times \exp\left(-\frac{0.129 - 1.5 \times 10^{-4} T}{k_B T}\right), \quad (14)$$

where  $k_B$  is the Boltzmann constant and  $T$  is the temperature (K). The frequency-dependent dielectric constant of metal in the visible and infrared regimes can be described by the following equation:<sup>37</sup>

$$\epsilon(\omega) = \epsilon_\infty - \sum_j \frac{\omega_{pj}^2}{\omega(\omega + i\gamma_j)} - \sum_j \frac{\Delta\epsilon_j \Omega_j^2}{\omega^2 - \Omega_j^2 + i\omega\Gamma_j}, \quad (15)$$

where  $\omega_{pj}$  is the plasma frequency,  $\gamma_j$  is the relaxation rate,  $\Omega_j$  is the resonant frequency,  $\Gamma_j$  is the damping constant, and  $\Delta\epsilon_j$  is the oscillator strength, where  $j$  is the number of interband transitions. The effective index  $n_{\text{eff}}$  can be related to the real part of the propagation constant  $n_{\text{eff}} = \text{Re}(\beta)$ .

### III. RESULTS

Figure 2 shows the effective indices and the imaginary parts of the propagation constants ( $\text{Imag}(\beta)$ ) versus the dielectric stripe thickness on the metal surface in the infrared regime. The width of the polyethylene layer is 600 nm, with its thickness changed from 20 to 2000 nm. Ag layer is adopted. The wavelength is 1.55  $\mu\text{m}$ . The fundamental mode (i.e.,  $\text{TM}_0$  mode) supported by the DLSPP waveguide structures has been investigated. The dashed line has been acquired by solving the transcendental Eq. (5). It is found from Fig. 2 that as the thickness of the dielectric stripe increases, the effective index increases.

It can be understood from the fact that when the dielectric stripe thickness  $d$  is very small, only a small fraction of the electric energy is stored in the dielectric stripe. As the polyethylene layer thickness increases, more energy penetrates into the dielectric stripe. As the thickness of the dielectric stripe further increases, most of the energy is stored in the dielectric ridge, and the propagation constants of the DLSPP modes reach a saturated value. This can be understood from the fact that the SPP modes are more affected by the metal/dielectric interface rather than by the dielectric stripe thickness. In addition, the results acquired by solving Eq. (5) are larger than those obtained from the TMM and FEM, due to the fact that the dielectric stripe width has not been considered by using the numerical methods. The FEM simulation is performed by using a commercial FEM software package-COMSOL MULTIPHYSICS 3.5. By using the proposed TMM, the width of the dielectric stripe can also be considered in the calculation, and the obtained results agree well with those from the FEM simulations, as shown in

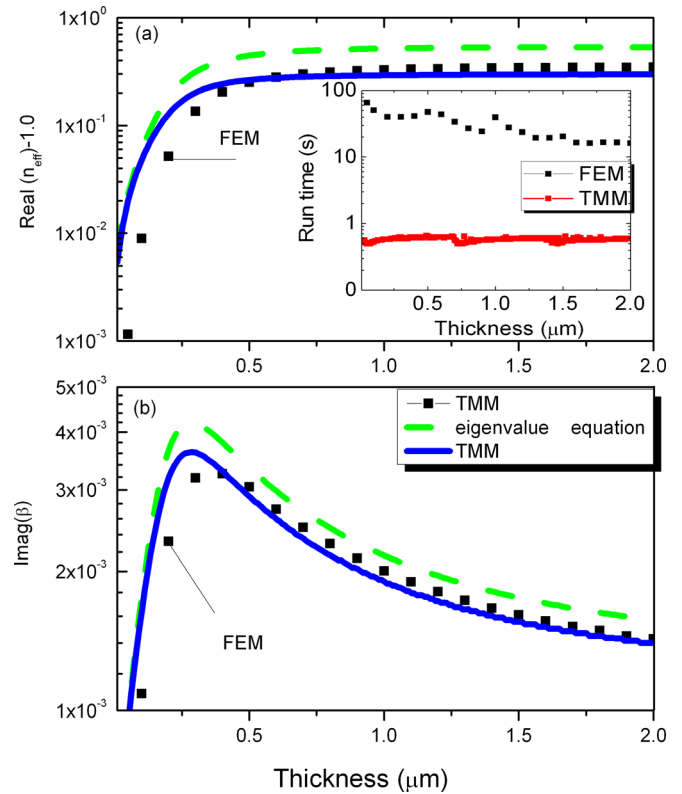


FIG. 2. The effective indices and  $\text{Imag}(\beta)$  of DLSPP modes as functions of the polyethylene stripe thickness. The results have been acquired by solving the eigenvalue equation, TMM and FEM, respectively. The inset in (a) shows the run time of the FEM and TMM. The wavelength is 1.55  $\mu\text{m}$ . The metal layer is Ag. The width of the polyethylene stripe is 600 nm.

Fig. 2. The results obtained from our TMM agree well with those given in other references. For instance, in Ref. 12 (the wavelength is 780 nm, the dielectric stripe is  $\text{SiO}_2$  with the refractive index of 1.45, and its thickness is 70 nm) the effective index of the SPPs mode is 1.15, and our TMM result gives 1.14. In another example, in Ref. 18 (the wavelength is 1.55  $\mu\text{m}$ , the thickness and the width of the dielectric stripe are both 600 nm) the effective index and the propagation length are 1.29 and 43  $\mu\text{m}$ , respectively; and the results from our TMM are 1.28 and 45  $\mu\text{m}$ , respectively. Further, the calculation speed of the proposed TMM is much faster than that of the FEM. The inset in Fig. 2(a) shows the run time versus the dielectric stripe thickness. The calculation time of the TMM is one or two orders shorter than that of FEM, e.g., if the dielectric thickness is 600 nm, the run time of FEM and TMM are  $\sim 43.92$  and 0.63 s, respectively. The RAM of our computer used is 4 Gbits.

Figure 3 shows the effective indices and the imaginary parts of propagation constants versus the dielectric stripe thickness on the metal surface in the THz regime. The width of the polyethylene layer is 100  $\mu\text{m}$  with its thickness from 60 to 120  $\mu\text{m}$ . The Cu layer is adopted. The frequency is 1 THz. The complex refractive index of Cu is  $2.10 \times 10^1 + 7.13 \times 10^1 i$  at 1 THz, which is taken from Ref. 38. It can be seen from Fig. 3 that as the dielectric stripe thickness increases, the effective index increases. Because the dielectric stripe width is not taken into account, the results obtained by solving Eq. (5) are larger than those from the TMM and FEM, as shown in Fig. 3. When

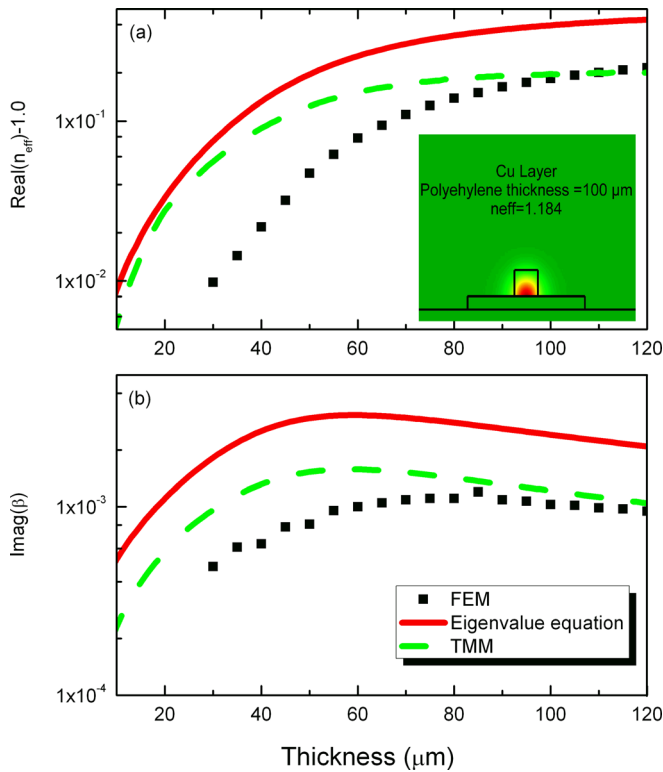


FIG. 3. The effective indices and  $\text{Imag}(\beta)$  of DLSP modes as the functions of the polyethylene stripe thickness. The results have been acquired by solving the eigenvalue equation, TMM and FEM. The frequency is 1.0 THz. The metal layer is Cu, and the polyethylene stripe width is  $100 \mu\text{m}$ . The inset shows the FEM simulation results of the Cu DLSPP waveguide structures.

TMM is adopted to investigate the DLSP waveguide and the width of the polyethylene stripe  $w_0$  is considered, the obtained numerical results are smaller than those of the FEM results. The reasons are as follows: the confinement of the optical mode of the dielectric stripe is not good; some of the modes leak out of the dielectric ridge, which can also be found from the FEM simulation results, as shown in the inset of Fig. 3. Therefore, we use the FWHM as the effective width of the optical mode, taking into account the parts of the modes leaking out of the dielectric stripe. Figure 3 shows that the results of the TMM are close to those obtained from FEM with the increase of the dielectric stripe width.

The propagation properties of the surface modes on the semiconductor layer can be easily modified by varying temperatures or doping concentrations. Figure 4 shows the effective indices and the propagation losses versus the thickness of the dielectric stripe. The width of the polyethylene layer is  $100 \mu\text{m}$ ; the thickness is changed from 60 to  $120 \mu\text{m}$ ; the temperature is 350 K; and the frequency is 1 THz. The inset of Fig. 4(b) displays the FEM simulation results of the semiconductor DLSP waveguide. Figure 4 shows that the propagation constants of the surface modes for InSb DLSP waveguides are larger than those of the metal DLSPs waveguide. In the THz regime, the dielectric constant of InSb is smaller than that of the metal. For example, the dielectric constants are  $-4.64 \times 10^3 + 2.99 \times 10^3 i$  and  $-9.58 \times 10^1 + 2.61 \times 10^2 i$  for Cu and InSb layer at 1 THz, respectively. The smaller dielectric constant of InSb results into the fact that there are more modes leaking into the InSb layer, leading to the increase of the skin depth and the propagation

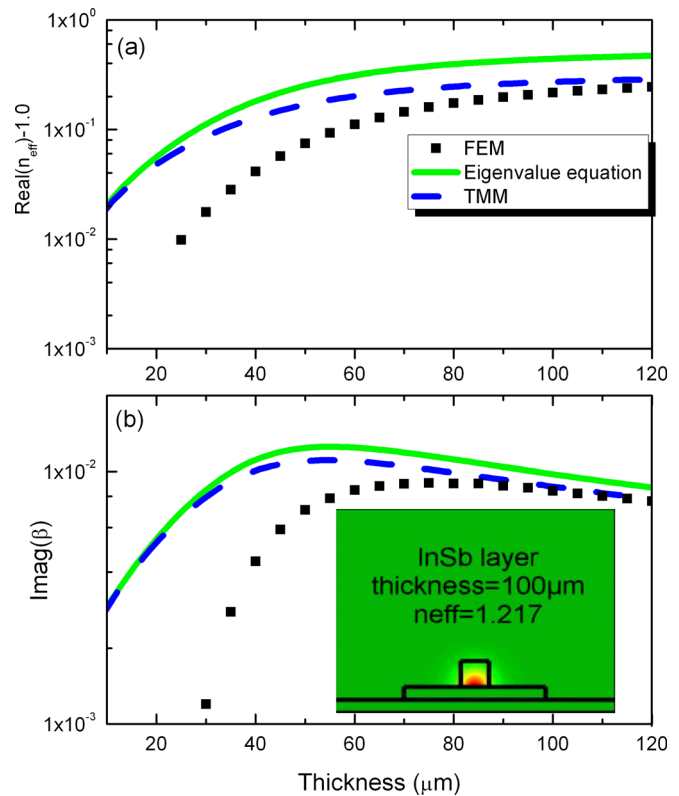


FIG. 4. The effective indices and  $\text{Imag}(\beta)$  of DLSPs modes as the functions of the thickness of the dielectric polyethylene stripe. The results have been acquired by solving the eigenvalue equation, TMM and FEM. The frequency is 1 THz. InSb layer is adopted. The width of the polyethylene stripe is  $100 \mu\text{m}$ . The inset shows the FEM simulation results of the semiconductor DLSP waveguides.

constant. For instance, at 1 THz the skin depths are  $0.67$  and  $1.92 \mu\text{m}$ , and the propagation constants of the surface modes are  $1.19 + 1.25 \times 10^{-3} i$  and  $1.27 + 8.88 \times 10^{-3} i$  for Cu and InSb DLSP waveguides, respectively. It should also be noted that the propagation constants of DLSP modes for the InSb DLSP structures are similar to those of metal DLSP waveguides in the infrared regime. For instance, at  $\lambda = 1.55 \mu\text{m}$  the dielectric constant of Ag is  $-1.20 \times 10^2 + 1.10 \times 10^1 i$  and the propagation constant is  $1.27 + 2.55 \times 10^{-3} i$ .

Due to the carrier concentration and the dielectric constant of InSb layer increase rapidly with the increase of temperature, not only the refractive index of the dielectric stripe, but also that of the semiconductor layer can be changed with the temperature. Therefore, sensors based on semiconductor DLSP waveguides show high sensitivity and more flexibility. The effective indices and  $\text{Imag}(\beta)$  of the surface modes versus the dielectric stripe thickness at different temperatures have been shown in Fig. 5. The results have been obtained from the TMM. The frequency is 1 THz. The thickness and width of the polyethylene stripe are both  $100 \mu\text{m}$ . We found that the calculation accuracy of the TMM is closed to that of the FEM. It is seen from Fig. 5 that as the temperature increases, the effective index decreases, and the propagation losses decrease. The carrier concentration of InSb increases with the increase of temperature, leading to the decrease of the dielectric constant. For example, at the temperatures of 300, 400, and 500 K, the carrier concentrations are  $1.96 \times 10^{16}$ ,  $10.39 \times 10^{16}$ , and

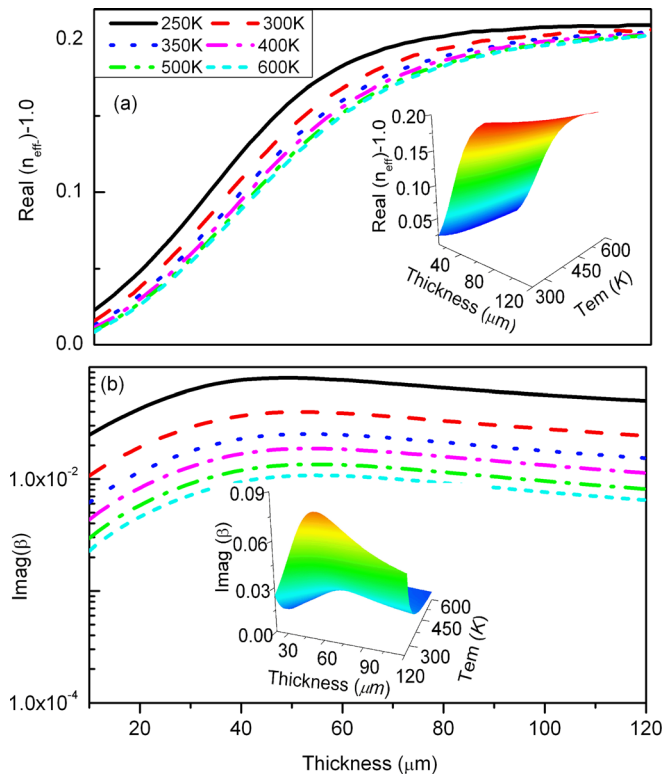


FIG. 5. The effective indices and  $\text{Imag}(\beta)$  of DLSP modes as the functions of the polyethylene stripe thickness at different temperatures. The results have been acquired by using the TMM. The frequency is 1 THz. The width and thickness of the polyethylene layer are both  $100 \mu\text{m}$ . The inset shows the effective indices and  $\text{Imag}(\beta)$  contour for the dielectric layer thickness and temperature.

$30.24 \times 10^{16} \text{cm}^{-3}$ , and the dielectric constants of InSb are  $-4.52 \times 10^1 + 1.16 \times 10^2 i$ ,  $-1.53 \times 10^2 + 4.73 \times 10^2 i$ , and  $-2.21 \times 10^2 + 9.90 \times 10^2 i$ , respectively. The carrier concentration and the dielectric constant of InSb are obtained from Eqs. (14) and (13), respectively. A larger dielectric constant of InSb at a higher temperature leads to a smaller skin depth, resulting in a decrease of the propagation constant. For instance, the skin depths are  $5.15$ ,  $2.64$ , and  $1.92 \mu\text{m}$ , and the propagation constants are  $1.2030 + 2.81 \times 10^{-2} i$ ,  $1.1990 + 1.33 \times 10^{-2} i$ , and  $1.1976 + 9.59 \times 10^{-3} i$  at the temperatures of 300, 400, and 500 K, respectively.

Most of the energy of SPP modes is localized at the interface between the metal (semiconductor) and the dielectric stripe, so the propagation properties of DLSP modes are greatly affected by the dielectric stripe. Figure 6 shows that the effective indices and the imaginary parts of the propagation constants of the surface modes versus the thickness of different kinds of dielectric stripe materials. The frequency is 1 THz. Cu and InSb substrate layers are adopted. The dielectric stripe width is  $30 \mu\text{m}$ . Polyethylene and quartz are deposited on the metal or InSb layers with the refractive indices of 1.52 and 1.98, respectively. It can be seen from Fig. 6 that with the increase of the refractive index of the dielectric stripe, both the effective indices and the propagation losses of the surface modes increase. For instance, when polyethylene and quartz are deposited on the Cu layers, the propagation constants are  $1.29 + 1.19 \times 10^{-3} i$  and  $1.53 + 2.38 \times 10^{-3} i$ , respectively. As the refractive index of the dielectric stripe

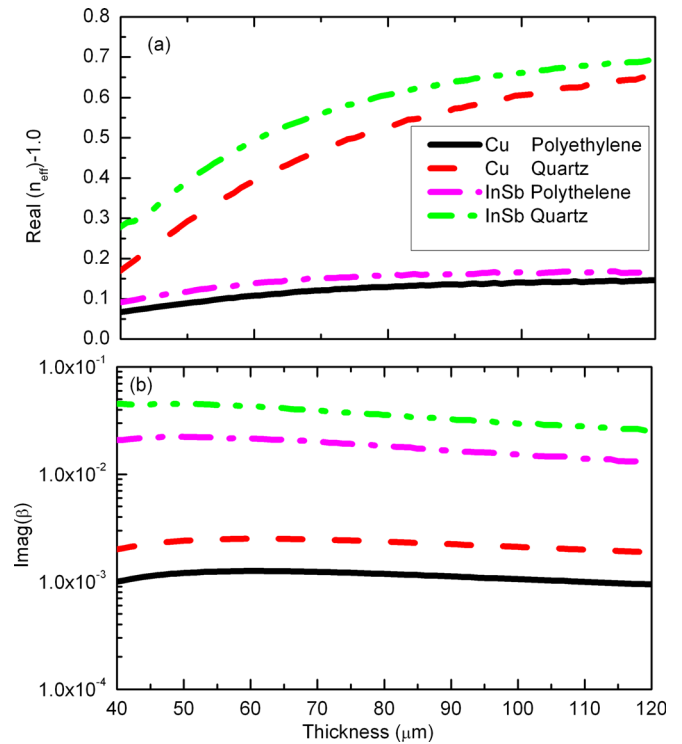


FIG. 6. The effective indices and  $\text{Imag}(\beta)$  of DLSP modes as the function of the dielectric stripe thickness. The dielectric stripes are polyethylene and quartz with the refractive indices of 1.52 and 1.98, respectively. The results have been acquired by using the TMM. The frequency is 1 THz. The width of the dielectric layer is  $80 \mu\text{m}$ .

increases, the modes can be better confined near the interface between metal (semiconductor) and dielectric stripe. The mode profile acquired from the FEM simulation is shown in Fig. 7, which shows that the mode can be well confined at the interface between metal (semiconductor) and dielectric stripe.

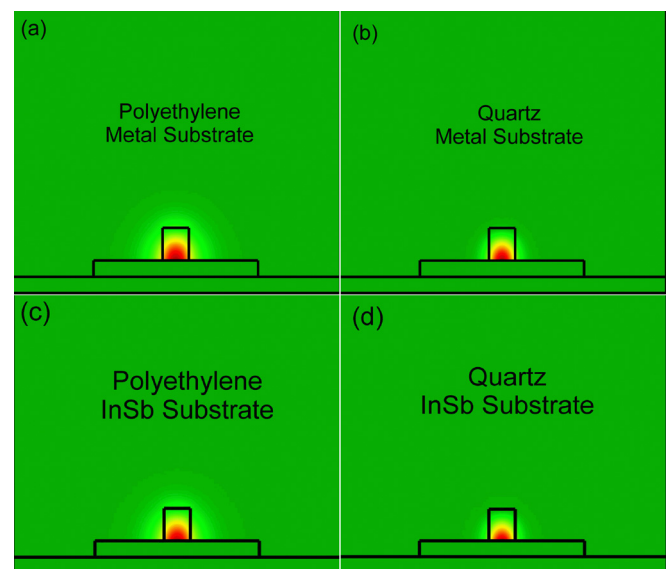


FIG. 7. The mode profiles of the DLSPs waveguide structures calculated by using the FEM software. The dielectric stripes in (a) and (c) are polyethylene, and quartz in (b) and (d). The substrate in (a) and (b) are Cu, and InSb in (c) and (d). The width of the dielectric stripe is  $80 \mu\text{m}$ , and the thickness is  $100 \mu\text{m}$ . The frequency is 1 THz.

#### IV. CONCLUSION

The propagation properties of DLSP waveguide structures in the THz and infrared regimes have been investigated by using the proposed TMM. The results obtained from the TMM are in good agreement with those from the FEM provided that the operating wavelength is compatible with the dielectric stripe width of the DLSPs waveguide. It is demonstrated that the TMM is an effective method to investigate the plasmonic waveguide structures, showing the merits of simplicity, as well as a much faster calculation speed, when compared to the FEM. As a case study, the waveguide properties of DLSPs structures in the THz and infrared regimes have been calculated and discussed. We believe that the proposed TMM method is a powerful and effective tool for simulation and optimization of DLSPs structures, and it is also broadly applicable to other various plasmonic devices.

#### ACKNOWLEDGMENTS

This work is supported by A\*STAR SERC under the Grant No. 082-101-0016 and Nanyang Technological University, Singapore under the Grant No. M58040017.

- <sup>1</sup>H. Raether, *Surface Plasmons on Smooth and Rough Surfaces and on Gratings* (Springer, Berlin, 1988).
- <sup>2</sup>W. L. Barnes, A. Dereux, and T. W. Ebbesen, *Nature (London)* **424**, 824 (2003).
- <sup>3</sup>Q. J. Wang, C. Yan, N. Yu, J. Unterhinninghofen, J. Wiersig, C. Pflügl, L. Diehl, T. Edamurac, M. Yamanishi, H. Kan, and F. Capasso, *Proc. Natl. Acad. Sci. U.S.A.* **107**, 22407 (2010).
- <sup>4</sup>N. Yu, Q. J. Wang, C. Pflügl, L. Diehl, F. Capasso, T. Edamura, S. Furuta, M. Yamanishi, and H. Kan, *Appl. Phys. Lett.* **94**, 151101 (2009).
- <sup>5</sup>C. L. Yan, Q. J. Wang, L. Diehl, M. Henstschel, J. Wiersig, N. Yu, C. Pflügl, F. Capasso, M. Belkin, T. Edamura, M. Yamanishi, and H. Kan, *Appl. Phys. Lett.* **94**, 241120 (2009).
- <sup>6</sup>R. F. Oulton, V. J. Sorger, D. A. Genov, D. F. P. Pile, and X. Zhang, *Nat. Photonics* **2**, 496 (2008).
- <sup>7</sup>X. Y. He, Q. J. Wang, and S. F. Yu, "Numerical study of gain-assisted terahertz hybrid plasmonic waveguide," *Plasmonics* (in press).
- <sup>8</sup>S. I. Bozhevolnyi, V. S. Volkov, E. Devaux, and T. W. Ebbesen, *Phys. Rev. Lett.* **95**, 046802 (2005).
- <sup>9</sup>X. Y. He, *Opt. Express* **17**, 15359 (2009).
- <sup>10</sup>X. Y. He, *J. Opt. A: Pure Appl. Opt.* **11**, 045708 (2009).
- <sup>11</sup>T. Holmgaard and S. I. Bozhevolnyi, *Phys. Rev. B* **75**, 245405 (2007).

- <sup>12</sup>J. Grandidier, S. Massenot, G. C. des Francs, A. Bouhelier, J. C. Weeber, L. Markey, A. Dereux, J. Renger, M. U. González, and R. Quidant, *Phys. Rev. B* **78**, 245419 (2008).
- <sup>13</sup>J. A. Kumar, J. Gosciniaik, T. B. Andersen, L. Markey, A. Dereux, and S. I. Bozhevolnyi, *Opt. Express* **19**, 2972 (2011).
- <sup>14</sup>J. Grandidier, G. C. des Francs, S. Massenot, A. Bouhelier, L. Markey, J. Weeber, C. Finot, and A. Dereux, *Nano Lett.* **9**, 2935 (2009).
- <sup>15</sup>A. C. Tasolamprou, D. C. Zografopoulos, and E. E. Kriezis, *J. Appl. Phys.* **110**, 093102 (2011).
- <sup>16</sup>O. Tsilipakos, T. V. Yioultsis, and E. E. Kriezis, *J. Appl. Phys.* **106**, 093109 (2009).
- <sup>17</sup>R. M. Briggs, J. Grandidier, S. P. Burgos, E. Feigenbaum, and H. A. Atwater, *Nano Lett.* **10**, 4851 (2010).
- <sup>18</sup>A. V. Krasavin and A. V. Zayats, *Appl. Phys. Lett.* **90**, 211101 (2007).
- <sup>19</sup>T. Gosciniaik, T. Holmgaard, and S. I. Bozhevolnyi, *J. Lightwave Technol.* **9**, 1473 (2011).
- <sup>20</sup>F. Yang, J. R. Sambles, and G. W. Bradberry, *Phys. Rev. B* **44**, 5855 (1991).
- <sup>21</sup>J. Grandidier, G. C. des Francs, L. Markey, A. Bouhelier, S. Massenot, J. C. Weeber, and A. Dereux, *Appl. Phys. Lett.* **96**, 063105 (2010).
- <sup>22</sup>C. C. Huang, *Opt. Express* **18**, 23711 (2010).
- <sup>23</sup>S. F. Yu, *IEEE J. Quantum Electron.* **39**, 1362 (2003).
- <sup>24</sup>N. F. Yu, Q. J. Wang, M. A. Kats, F. A. Fan, S. P. Khanna, L. H. Li, A. G. Davies, E. H. Linfield, and F. Capasso, *Nat. Mater.* **9**, 730 (2010).
- <sup>25</sup>Q. J. Wang, C. Yan, L. Diehl, M. Henstschel, J. Wiersig, N. F. Yu, C. Pflügl, M. A. Belkin, T. Edamura, M. Yamanishi, H. Kan, and F. Capasso, *New J. Phys.* **11**, 125018 (2009).
- <sup>26</sup>J. C. Cao, *Phys. Rev. Lett.* **91**, 237401 (2003).
- <sup>27</sup>M. Belkin, Q. J. Wang, C. Pflügl, A. Belyanin, S. P. Khanna, A. G. Davis, E. Linfield, and F. Capasso, *IEEE J. Sel. Top. Quantum Electron.* **15**, 952 (2009).
- <sup>28</sup>R. W. Adams, K. Vijayraghavan, Q. J. Wang, J. Fan, F. Capasso, S. P. Khanna, A. G. Davies, E. H. Lin, and M. A. Belkin, *Appl. Phys. Lett.* **97**, 131111 (2010).
- <sup>29</sup>X. Y. He, *J. Opt. Soc. Am. B* **26**, A23 (2009).
- <sup>30</sup>X. Y. He, *J. Opt. Soc. Am. B* **27**, 2298 (2010).
- <sup>31</sup>N. Yu, Q. J. Wang, and F. Capasso, *Laser Photonics Rev.* **6**, 24 (2012).
- <sup>32</sup>I. P. Kaminow, W. L. Mammel, and H. P. Weber, *Appl. Opt.* **13**, 396 (1974).
- <sup>33</sup>A. Tesár and L. Fillo, *Transfer Matrix Method* (Kluwer, Dordrecht, The Netherlands, 1988).
- <sup>34</sup>S. W. Gao, "Electron kinetics in terahertz quantum cascade laser," Ph.D. dissertation (Chinese Academy of Science, Beijing, 2004).
- <sup>35</sup>M. A. Ordal, R. J. Bell, R. W. Alexander, L. L. Long, and M. R. Querry, *Appl. Opt.* **24**, 4493 (1985).
- <sup>36</sup>M. Oszwaldowski and M. Zimpel, *J. Phys. Chem. Solids* **49**, 1179 (1988).
- <sup>37</sup>S. G. Rodrigo, F. J. García-Vidal, and L. Martín-Moreno, *Phys. Rev. B* **77**, 075401 (2008).
- <sup>38</sup>E. D. Palik, *Handbook of Optical Constants of Solids* (Academic, New York, 1985).